Informes Técnicos Ciemat

776
Diciembre 1995

# Electron beam test of an iron/gas calorimeter based on ceramic parallel plate chambers

A. Arefiev
Gy. L. Bencze
A. Bizzeti
E. Choumilov
C. Civinini
F. Dalla Santa
R. D'Alessandro
A. Ferrando
M.C. Fouz
A. Herve
A. Iglesias
V. Ivochkin
M.I. Josa
F. Maggi
A. Malinin
M. Meschini
V. Pojidaev
E. Radermacher
J.M. Salicio

**Instituto de Investigación Básica**

Toda correspondencia en relación con este trabajo debe dirigirse a la Unidad de Gestión de Recursos de la Información, Centro de Investigaciones Energéticas, Medioambientales y Tecnológicas, Ciudad Universitaria, 28040-MADRID, ESPAÑA.

Las solicitudes de ejemplares deben dirigirse a esta misma unidad.

Los descriptores se han seleccionado del Thesauro del DOE para describir las materias que contiene este informe con vistas a su recuperación. La catalogación se ha hecho utilizando el documento DOE/TIC-4602 (Rev. 1) Descriptive Cataloguing On-Line, y la clasificación de acuerdo con el documento DOE/TIC.4584-R7 Subject Categories and Scope publicados por el Office of Scientific and Technical Information del Departamento de Energía de los Estados Unidos.



**Depósito Legal:** M-14226-1995
**NIPO:** 238-95-010-2
**ISSN:** 0214-087X

Editorial CIEMAT

CLASIFICACIÓN DOE Y DESCRIPTORES

440500
CALORIMETERS, ELECTRONS, ELECTRON BEAMS, ENERGY RESOLUTION, TESTING, DATA ANALYSIS, MONTE CARLO METHOD

**"Electron beam test of an iron/gas calorimeter based on ceramic parallel plate chambers".**

Arefiev, A.; Bencze, Gy.L.; Bizzeti, A.; Choumilov, E.;
Civinini, C.; Dalla Santa, F.; D'Alessandro, R.; Ferrando, A.;
Fouz, M.C.; Herve, A.; Iglesias, A.; Ivochkin, V.; Josa, M.I.;
Maggi, F.; Malinin, A.; Meschini, M.; Pojidaev, V.;
Radermacher, E.; Salicio, J.M.
35 pp. 14 figs. 23 refs.

## Abstract

The baseline option for the very forward calorimetry in the CMS experiment is an iron/gas calorimeter based on parallel plate chambers. A small prototype module of such a calorimeter, has been tested using electrons of 5 to 100 GeV/c momentum with various high voltages and two gases: $CO_2$ (100%) and $CF_4/CO_2$ (80/20), at atmospheric pressure. The collected charge has been measured as a function of the high voltage and of the electron energy. The energy resolution has also been measured. Comparisons have been made with Monte-Carlo predictions. Agreement between data an simulation allows to make and estimation of the expected performance of a full size calorimeter.

**"Pruebas en haces de electrones de un calorímetro de hierro/gas basado en cámaras de gas de planos paralelos".**

Arefiev, A.; Bencze, Gy.L.; Bizzeti, A.; Choumilov, E.;
Civinini, C.; Dalla Santa, F.; D'Alessandro, R.; Ferrando, A.;
Fouz, M.C.; Herve, A.; Iglesias, A.; Ivochkin, V.; Josa, M.I.;
Maggi, F.; Malinin, A.; Meschini, M.; Pojidaev, V.;
Radermacher, E.; Salicio, J.M.
35 pp. 14 figs. 23 refs.

## Resumen

La opción de base para la calorimetría a pequeño ángulo de CMS es un calorímetro de hierro/gas basado en cámaras de gas de planos paralelos. Un módulo calorimétrico prototipo ha sido probado utilizando haces de electrones de impulsiones comprendidas entre 5 y 100 GeV/c, con varios valores para el alto voltaje y utilizando como gases: $CO_2$ (100%) y $CF_4/CO_2$ (80/20) a presión atmosférica. La carga recogida ha sido medida en función del voltaje y de la energía de los electrones incidentes. También ha sido medida la resolución de la energía. Se han hecho comparaciones con las predicciones Monte-Carlo. El acuerdo entre datos y simulaciones permite hacer una estimación de las prestaciones esperadas para un calorímetro de dimensiones reales.

## 1. Introduction

Among the aims of the CMS experiment [1] are an accurate measurement of the missing energy as well as a good forward jet tagging and reconstruction. A calorimetry with full solid angle coverage for best missing energy measurement is essential for instance for any search of new types of particles giving a relatively large amount of missing energy, such as supersymmetric particles. A good forward jet tagging and reconstruction will allow the study of interesting events like the V-V fusion process (with or without Higgs production).

From simulation studies [2,3], the calorimeters in the very forward region of CMS need to have a modest energy resolution, a stochastic term in the order of $100\%/\sqrt{E}$ and a small constant term, for single hadrons, a good electron/pion compensation (essential to the measurement of the correct jet energy) and a fine granularity to tag and reconstruct forward jets. The granularity is also needed to reject fake jets formed by particles coming from superimposed minimum bias events and for adequate jet angular resolution in the transverse plane.

The technical requirements for calorimeters extending the pseudorapidity coverage up to 5 units are very demanding. The device should be fast, work in areas of very high occupancy [4], under high radiation levels [5, 6] and be simple, robust and unexpensive.

A very forward calorimeter (VF), based on parallel plate chambers (PPC) [7], has been proposed [8] for the CMS experiment.

In a recent paper we have presented a solution for the VF based on parallel plate volumes (PPV) [9]. PPVs are small and rigid modules made of machined thick iron plates, where the absorber forms, at the same time, the electrodes [10] of the PPCs. As shown in ref. [9] the test beam results confirmed the validity of this solution.

We present now the baseline option [1] for CMS: a very forward calorimeter, having iron plates as absorber and planes of ceramic parallel plate chambers (intermixed with the Fe-plates) as active medium. The design guarantees the best possible granularity achieved using small detector elements arranged in a tower structure. It gives, at the same time, the maximum flexibility in the sampling choice from the individual PPCs.

In addition, we present results obtained with a small prototype having an equivalent depth of $\approx 22\ X_0$ placed on an electron beam.

The paper is organized as follows. Section 2 explains the PPC working principle. Construction and technology of the ceramic chambers are given in section 3. The general lines of the proposed

VF/PPC solution for CMS are drawn in section 4. The test beam experimental set-up is given in section 5. The results are presented in sections 6 and 7, while in section 8 the comparison between Monte Carlo prediction and data is made. Conclusions are drawn in section 9.

## 2. The detector cells working principle

A Parallel Plate Chamber is a gaseous detector [7,11] with planar electrodes, working in the avalanche mode. A single chamber consists of two planar metal (or metallized) electrodes kept at a fixed distance by a spacer. The gap between the electrodes is very small (in this application 1.5 mm with an accuracy of 5 μm) and is filled with gas which, in our case, is at atmospheric presure. When a high voltage is applied between the electrodes, a uniform and intense electric field is established inside the detector sensitive volume.

The operating principle is shown in fig. 1. Due to the intense electric field a primary ionization electron starts immediately an avalanche multiplication process. For this reason PPC time jitter is negligible with respect to that of usual wire chambers.

The electrons are collected at the anode, and the cloud of positive ions drift towards the cathode. The motion of electrons in the avalanche induces a fast (< 1 ns) [12] signal on the electrodes which is followed by a much slower one (≈ 3 μs) due to the motion of the ions.

The number of electrons collected by the anode is given [13] by

$$n = n_0 e^{\alpha x} \tag{1}$$

where $n_0$ is the number of primary electrons at a given distance x from the anode and a is the first Townsend coefficient. The gas gain (ratio between total collected charge and primary ionization) is

$$G = e^{ax} \tag{2}$$

and the average gain for high energy particles is

$$M = e^{\alpha d}/\alpha d \tag{3}$$

where d is the distance between the electrodes.

The maximum gas gain is $e^{\alpha d}$. Due to the exponential development of the avalanches and their different lengths, the gas

amplification depends strongly on the distribution of the primary ionization charge inside the chamber. Therefore the total collected charge depends not only on the amount of the primary ionization but also on where it is located; as a consequence, the charge spectrum for single minimum ionizing particles crossing the detector perpendicularly to the electrodes is not a Landau distribution.

The space charge effect, limiting conventional wire chambers efficiency in an intense beam, is much less important in a PPC. In fact, in a wire chamber the avalanche development is restricted to a very small space region close to the anode, while in a PPC the large lateral extension of the avalanche greatly reduces the charge density, increasing its capability to work at very high rates.

The general properties of the PPCs have been discussed elsewhere [14 - 18]. Among the possible technologies for building these detectors, we consider here the use of thin ceramic chambers.

## 3. The ceramic PPC construction and technology

In fig. 2 a schematic drawing of the ceramic PPC components is shown. A PPC unit consists of two ceramic plates with evaporated chromium electrodes separated by a ceramic frame that close the chamber and whose thickness determines the gas gap. Ceramic (97% alumina) is machined by polishing to a planarity and parallelism better than 5 μm. Both electrode plates and frame plate are machined in the same way. The internal part of the frame plate can then be cut by laser, by water-jet or by diamond saw.

Grooves with a rounded edge made on the electrode plates are needed to prevent the rise of the electric field intensity near the border of the electrode. The open ends of the grooves also provide the way for gas exchange. The small holes drilled near the corners of the plates hold the feedthroughs for the electric contact with the thin metallized surface of the electrode plates. The chromium layer has 0.5 μm thickness and the outer border of the metallization stops in the middle of the grooves. In fig 3 technical drawings for the construction of the ceramic electrodes and frame are shown. All chamber components used in this work have been produced, with the same technique and following the design in fig. 3, by two companies, one from West [19] and the other from East Europe [20]. Sample of cells obtained from both companies perform equally well and they differ mainly on the price.

## 4. The VF/PPC solution for CMS

Big surface coverage is obtained by use of a multicell structure, to which PPCs, having flexibility of geometrical shape, adapt well. It is also much easier to produce components with good mechanical accuracy for small cells than for big ones. Each cell in a multicell detector plane is almost mechanically independent from the others, except for high voltage, signal and ground connections that, in general, will be fixed on an assembly printed board.

One possible mechanical arrangement for the VF/PPC is shown in fig. 4. It consists of four large modules of approximate dimensions 165 x 135 x 330 $cm^3$ on each side of the interaction point, leaving a central hole $\approx$ 30x30x330 $cm^3$, for the beam pipe. The front face is located at about 11 m up and downstream of the CMS interaction point, covering the pseudorapidity region $3.0 \leq |\eta| \leq 5.0$. A module consists of 60 planes of parallel plate chambers interleaved with plates of 35 mm thick iron absorber.

Each PPC plane in a module contains around 700 cells in a compact box about 2 cm thick. Towers closest to the beam ($3.5 \leq |\eta| \leq 5.0$) have transverse size 5 x 5 $cm^2$, while outer towers may have 10 x 10 $cm^2$. This granularity is adequate for jet finding and transverse angle reconstruction [3] and keeps the occupancy due to the minimum bias pileup [4] down to the required level. About 350000 PPCs (5 x 5 $cm^2$) are needed to fully equip both VF/PPC sides. The gas gap in a PPC is 1.5 mm. The VF/PPC has three-fold segmentation in depth.

The total depth of the VF/PPC is about 3.3 m (equivalent absorber length $\approx 12\ \lambda_I$). For pions of 1 TeV, simulation show [21] that shower leakage is less than 2%. Each iron plate weighs 570 kg and the VF/PPC on each side of the interaction point weighs about 140 tonnes.

The front-end electronics is located at the outer surface of the calorimeter. This arrangement is necessary to keep electronics safely away from the high neutron flux ($\approx 10^8\ cm^{-2}\ s^{-1}$) expected when running at the highest luminosity [6].

## 5. Experimental test beam set-up

### *5.1 The prototype*

We have constructed an iron/PPC calorimeter prototype consisting of 13 PPC planes interleaved with 30 mm iron plates used as absorber. A sketch of the prototype is shown in fig. 5.

Total length was equivalent to about 22 $X_0$. The PPC cells have been assembled on one side of a printed circuit board (50 x 50 $cm^2$) inside a clean gas tight box where the gas is circulating. On the top of the enclosing box there is a HV distribution system that feeds each chamber with a single line. Each cell has a blocking capacitor and resistor which connect it to the HV supply. Also on top of the PPC box are placed the signal connectors. From there, 2.5 m long twisted pair cables bring the signals to the associated front end electronics. In this first prototype, planes of only 3 x 3 PPCs (as indicated in fig. 5) were used covering a surface of 15 x 15 $cm^2$. Place is available for up to 8 x 8 PPCs per plane.

*5.2 Experimental setup*

The module was exposed to electron beams from the CERN SPS (X5 beam, electron energy range from 5 to 100 GeV). Unfortunately there was no way to monitor the beam impact point on the calorimeter. In fact the beam straddled two PPCs thus worsening the energy resolution due to dead spaces between detectors.

The data were taken at four voltages (5100, 5200, 5300 and 5400 V) using pure $CO_2$ and at 5550 V and 5600 V using $CF_4/CO_2$ (80/20).

The gases were at atmospheric pressure. The gas system consisted of a pressure reductor that sends the gas into the prototype through a flowmeter, a filter (removing dust particles down to 0.5 μm) and a trap for oxigen and water molecules. The final content in $O_2$ and $H_2O$ in the gas gap was smaller than 10 ppm.

The amplifiers have 15 ns rise time, a gain of 2 x 9 mV/μA and an electric noise of about 15000 $e^-$ using the 2.5 m input cable.

From the preamplifier boards, 80 m long shielded twisted pairs cables (32 channels/cable) bring the different signals to the Fastbus ADCs LRS 1882F (see fig. 6). Data was written to disk and tape through a Motorola MVME 167-002 CPU. Data taking and online monitoring were done with an HP 9000-712 work station.

## 6. Collected charge as function of the high voltage

Typical total charge spectra for 100 GeV electrons are shown in figs. 7 a) and b) for pure $CO_2$ and $CF_4/CO_2$ (80/20) gas mixture at 5300 and 5600 V respectively. The curves are the results of Gaussian fits to the data.

The mean values of the charge distributions (coming from the Gaussian fits) are shown in fig. 8 as a function of the HV, for various electron energies using $CO_2$. They all show the expected exponential behaviour. The error bars include both statistical and sistematics (mainly coming from gas density variations).

## 7. Linearity and energy resolution

The average collected charge (obtained from a Gaussian fit) is plotted in figs. 9 a) and b) as a function of the electron energy, for $CO_2$ and $CF_4/CO_2$ respectively, for different HV values. The response is linear with the energy in all cases. The straight lines in the plots represent the corresponding fits to the data. The slopes increase with the high voltage for both gases and are found to be:

$$\langle Q\ (fC)\rangle = (50 \pm 2)\ E\ (GeV) \qquad \text{at } 5200\ V$$
$$\langle Q\ (fC)\rangle = (120 \pm 5)\ E\ (GeV) \qquad \text{at } 5300\ V$$
$$\langle Q\ (fC)\rangle = (240 \pm 8)\ E\ (GeV) \qquad \text{at } 5400\ V$$

for $CO_2$, and

$$\langle Q\ (fC)\rangle = (42 \pm 3)\ E\ (GeV) \qquad \text{at } 5550\ V$$
$$\langle Q\ (fC)\rangle = (91 \pm 5)\ E\ (GeV) \qquad \text{at } 5600\ V$$

in the case of $CF_4/CO_2$.

Finally, the energy resolution $\sigma(E)/\langle E\rangle$, as a function of $1/\sqrt{E}$, is given in fig. 10 a) and b) for $CO_2$ and $CF_4/CO_2$ respectively, for various high voltages, after subtracting in quadrature the contribution of the electronic noise. We have fitted the data points to the form

$$\sigma(E)/E = a/\sqrt{E} + c \qquad (4)$$

and obtained:

$$\sigma(E)/E = (1.16 \pm 0.17)/\sqrt{E} + (0.02 \pm 0.02) \qquad \text{at } 5200\ V$$
$$\sigma(E)/E = (0.96 \pm 0.14)/\sqrt{E} + (0.03 \pm 0.02) \qquad \text{at } 5300\ V$$
$$\sigma(E)/E = (1.00 \pm 0.20)/\sqrt{E} + (0.02 \pm 0.02) \qquad \text{at } 5400\ V$$

for $CO_2$, and

$$\sigma(E)/E = (0.87 \pm 0.15)/\sqrt{E} + (0.02 \pm 0.02) \qquad \text{at } 5550\ V$$
$$\sigma(E)/E = (0.82 \pm 0.13)/\sqrt{E} + (0.03 \pm 0.02) \qquad \text{at } 5600\ V$$

for the mixture $CF_4/CO_2$.

## 8. Comparison with Monte-Carlo predictions

### *8.1 Monte-Carlo simulation*

For cascade simulation, we have used a geometry consisting on 35 iron plates of dimensions 500 x 500 x 30 $mm^3$ interleaved with PPC layers. Each PPC layer consists of a 8 x 8 matrix of ceramic PPCs. Each PPC cell is made of two ceramic plates 50 x 50 x 2 $mm^3$ with a 1.5 mm gap of gas. The active volume of gas in a cell has 47 x 47 $mm^2$ transverse dimensions. The distance between the sides of two adjacent cells is 2 mm. this geometry reproduces almost exactly the layout shown in fig. 5.

GEANT 3.21 [22] was used to generate showers in the simulated module.

Since, as said in section 2, in the avalanche mode the number of collected electrons depends on the distance between the primary ionization and the anode (for a given gas at constant temperature and pressure), we have divided each of the 1.5 mm gas gaps into 10 GEANT independent subvolumes of 0.15 mm each. Information about dE/dx in the gas subvolumes was written on disk for a subsequent simulation of the avalanche operation.

Under these conditions we have simulated some 1000 electron showers for each considered energy point. The simulation is done only for the $CF_4/CO_2$ gas mixture.

### *8.2 Simulation of the avalanche mode of operation*

Using the information provided by GEANT on the energy deposited by ionization, $\Delta E_i$, in each of the 10 subvolumes of a given gas gap, we have approximated the expected number of electrons collected at the anode, in eq. (1), by:

$$N = \Sigma\, n_p^i\, e^{\alpha x_i} \qquad (5)$$

where $n_p^i$ is the expected primary electron-ion production, $\alpha$ is the first Townsend coefficient and $x_i$ is the distance from the middle of the i-th subgap gas to the anode. This process is repeated for any $\Delta E_i$ in the gas. The values of the First Townsend coefficient used in the various simulations were taken from ref [23].

*8.3 Comparison of experimental and Monte-Carlo data*

Fig. 11 shows, as an example, the collected charge distributions, normalized to one, for the data (dashed line) and for the Monte-Carlo prediction (continuous line) for 60 and 80 GeV electrons in the case of $CF_4/CO_2$ at 5600 V. Data and Monte Carlo (within the limited simulated statistics) agree well.

The comparison of measured and predicted average collected charges as a function of the electron energy are shown in figs. 12 a) and b), together with their respectives straight line fits, for the case of $CF_4/CO_2$ at 5550 V and 5600 V respectively. Both sets of values show a good agreement. The fitted functions (to be compared with the ones given in section 7) are:

$$\langle Q\ (fC)\rangle = (41.22 \pm 0.01)\ E\ (GeV) \qquad \text{for 5550 V}$$
$$\langle Q\ (fC)\rangle = (90.42 \pm 0.03)\ E\ (GeV) \qquad \text{for 5600 V}$$

Finally, we compare measured and predicted energy resolutions figs. 13 a) and b) for the same above experimental conditions. Predictions are:

$$\sigma(E)/E = (0.90 \pm 0.04)/\sqrt{E} + (0.01 \pm 0.01) \qquad \text{for 5550 V}$$
$$\sigma(E)/E = (0.84 \pm 0.04)/\sqrt{E} + (0.01 \pm 0.01) \qquad \text{for 5600 V}$$

The agreement in the slope between data (see section 7) and Monte Carlo is indeed very good.

The general agreement between data and simulation allows us to make preliminary predictions of the performance of a full VF/PPC as described in section 4. We obtain:

$$\sigma(E)_e/\langle E\rangle_e = (0.99 \pm 0.09)/\sqrt{E} + (0.01 \pm 0.01) \text{ and}$$
$$\sigma(E)_\pi/\langle E\rangle_\pi = (1.08 \pm 0.10)/\sqrt{E} + (0.03 \pm 0.01).$$

## 9. Conclusions

We have presented the general outlines for a very forward calorimeter based on ceramic parallel plate chambers, proposed for the low angle regions of the CMS experiment.

A prototype module of such a calorimeter was tested at the CERN SPS X5 electron beam.

We have observed that this type of calorimeter has a linear response. We have measured the energy resolution of this prototype and compared it to our Monte Carlo predictions. Energy resolutions ranging from $1.16/\sqrt{E} + 0.02$ to $0.82/\sqrt{E} + 0.03$ were

measured and all the data show good agreement with Monte Carlo expectations.

Having demonstrated the feasibility of the mechanical construction using only radiation resistant materials, the smooth operation of the device and the fast collection of the signal, we conclude that the proposed solution fulfills the basic physics and technological requirements for a very forward calorimeter in the CMS experiment. Upsizing of the actual prototype dimensions to full containment of hadron cascades is necessary so as to have a direct check of the Monte Carlo expectations concerning the single pion energy resolution.

**Acknowledgements**

This work has been supported by the following organizations and funding agencies: CERN, Geneva, Switzerland, CIEMAT, Madrid, Spain; CICYT, Spain; INFN, Firenze, Italy; Accademy of Sciences, Hungary and ITEP, Moscow, Russia.

We acknowledge useful discussions and help from, M. Aguilar-Benitez, J. Bourotte, Yu. Galaktionov, M. Haguenauer, L. Martinez-Laso and T.S. Virdee.

We also acknowledge the technical support from the CERN staff (in and out CMS Group), the mechanical workshops of CIEMAT and the help from I. Melnikov, V. Plotnikov and A. Pardillo, in the construction of the VF/PPC prototype.

## References

[1] The CMS Collaboration, CERN/LHCC 94-38, LHCC/P1 (1994).
[2] A. Ferrando et al., CMS Technical Note TN/95-037 (1995).
[3] A. Ferrando et al., CMS Technical Note TN/95-061 (1995).
[4] C. Burgos et al., CMS Technical Note TN/95-035 (1995).
[5] G. R. Stevenson et al., CERN/TIS-RP/IR/92-06 (1992).
[6] A. Ferrando et al., Nucl. Instr. and Methods B 83 (1993) 205.
[7] Yu. Galaktionov et al., Nucl. Instr. and Methods A 317 (1992) 116.
[8] M. C. Fouz et al., CERN/DRDC 93-43, DRDC/P51 (1993).
[9] A. Arefiev et al., Nucl. Instr. and Methods A 364 (1995) 133.
[10] A. Bizzeti et al., Nucl. Instr. and Methods A 335 (1993) 102.
[11] A. Arefiev et al., Nucl. Instr. and Methods A348 (1994) 318.
[12] A. Arefiev et al., Nucl. Phys. B (Proc. Suppl.) 32 (1993) 223.
[13] J.S. Townsend, Nature 62 (1900) 340 and Phil. Mag. 1 (1901) 198.
[14] A. Ferrando et al., CMS Technical Note TN/92-23 (1992).
[15] A. Arefiev et al., RD5 Technical Note TN/92-04 (1992).
[16] V. Akimov et al., Nucl. Instr. and Methods A 334 (1994) 120.
[17] A. Arefiev et al., CERN PPE/93-82 (1993).
[18] The Parallel Plate Chambers Collaboration, CMS Technical Note TN/94-159 (1994).
[19] Guinchard SA, 5 Ruelle Vautier, c.p. 237, 1400 Yverdon-les-Bains, Switzerland.
[20] Electronic Integral Systems, 1-37 Pochtamtskaya, 190000 St. Petersburg, Russia.
[21] A. Ferrando et al., CMS Technical Note TN/93-81 (1993).
[22] R. Brun et al., CERN DD/EE/84-1 (1987). See also CERN Program Library Long Writeup W5013 (1993).
[23] A. Arefiev et al., CERN PPE/93-82 (1993).

## Figure captions

Fig. 1: The PPC working principle.
Fig. 2: Schematic drawing of the components of a ceramic PPC.
Fig. 3: Technical drawings for the construction of the ceramic PPCs:
a) electrodes,
b) frame.
Fig. 4: Layout of the proposed VF/PPC for CMS.
Fig. 5: Sketch of the calorimeter module prototype.
Fig. 6: Sketch of the signal readout.
Fig. 7: Charge distributions (in fC) for 100 GeV electrons:
a) $CO_2$ at 5300 V,
b) $CF_4/CO_2$ (80/20) at 5600 V.
Fig. 8: Collected charge as a function of the high voltage for various electron energies ($CO_2$).
Fig. 9: Collected charge as a function of the electron energy for various high voltages:
a) $CO_2$,
b) $CF_4/CO_2$ (80/20).
Fig.10: Energy resolution for electrons as a function of $1/\sqrt{E}$ for various high voltages:
a) $CO_2$,
b) $CF_4/CO_2$ (80/20).
Fig. 11: Normalized charge distributions for the data (dashed line) and for the Monte Carlo prediction (continous line) for 60 and 80 GeV electrons in the case of $CF_4/CO_2$:
a) at 5550 V,
b) at 5600 V.
Fig. 12: Comparison of measured (full circles) and predicted (open circles) collected charge as a function of the electron energy, with their corresponding straight line fits, for the $CF_4/CO_2$ gas mixture:
a) at 5550 V,
b) at 5600 V.
Fig. 13: Comparison, for the $CF_4/CO_2$ gas mixture, of the measured (open triangles) and the predicted (open circles) energy resolutions, with their corresponding fits (see text).
a) at 5550 V,
b) at 5600 V.

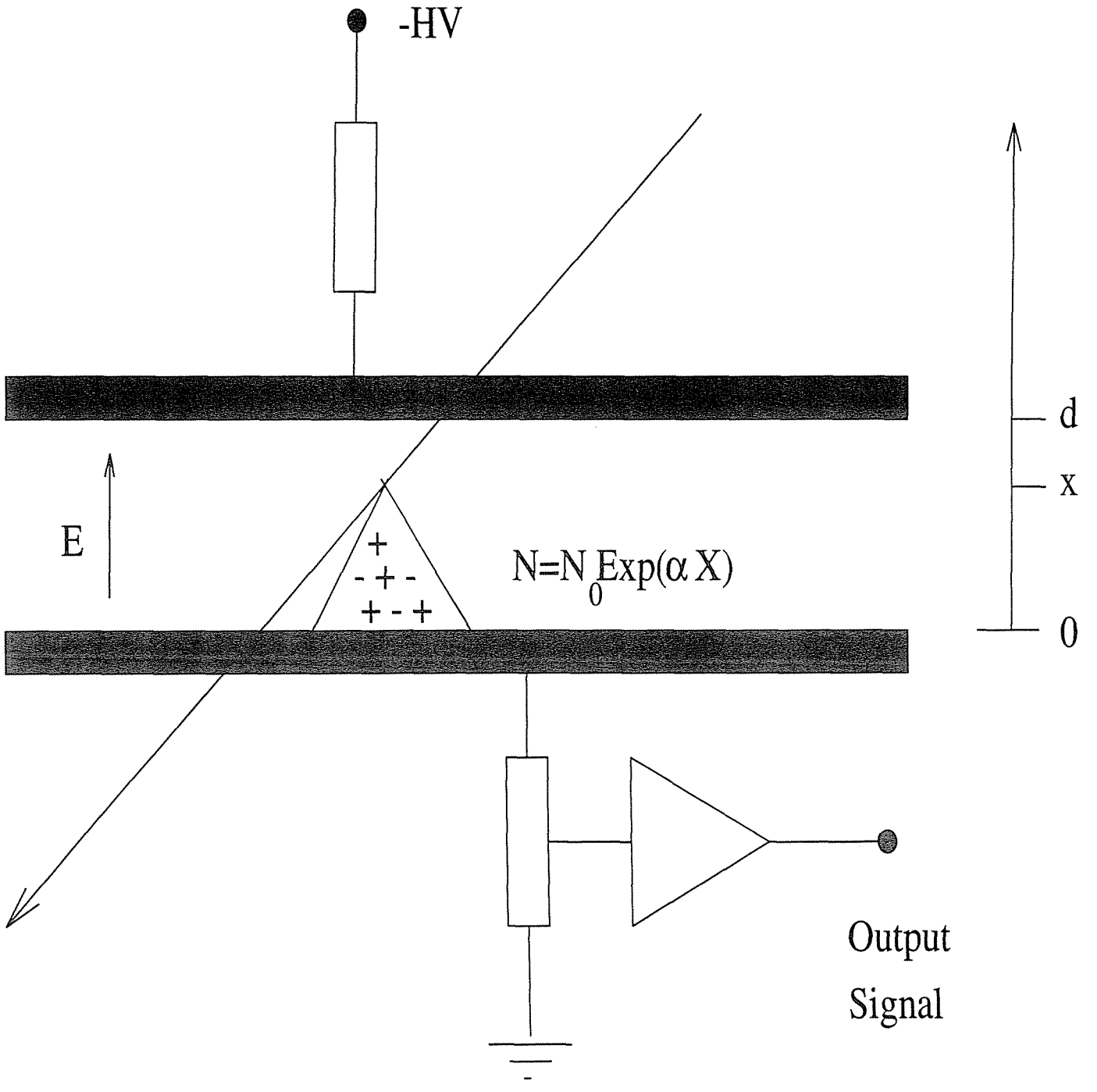


**Fig. 1**

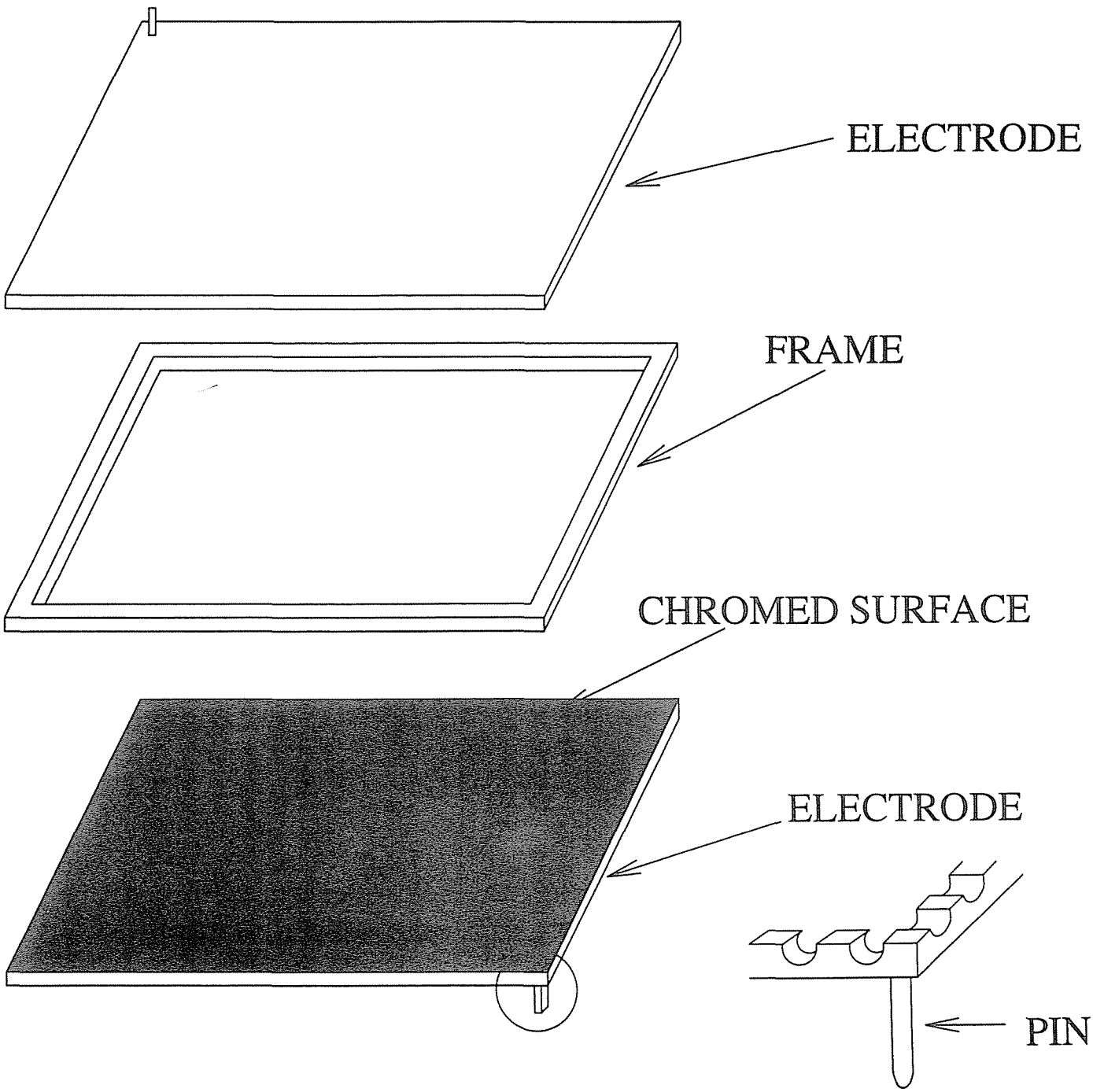


**Fig. 2**

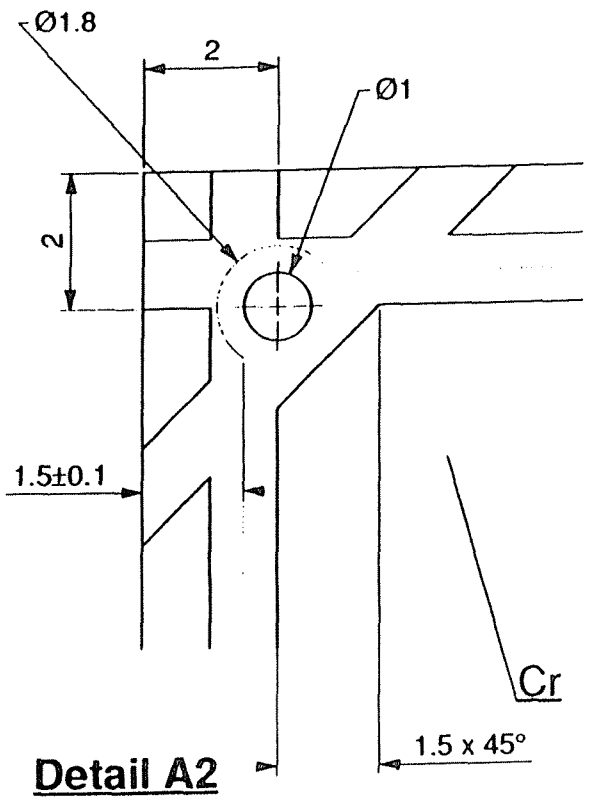


**Detail A2**
Ech. 10/1

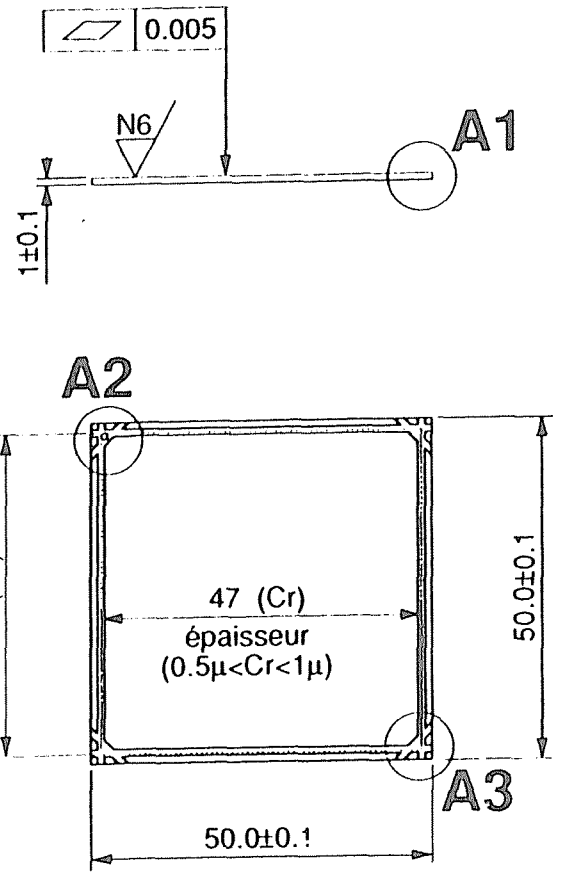


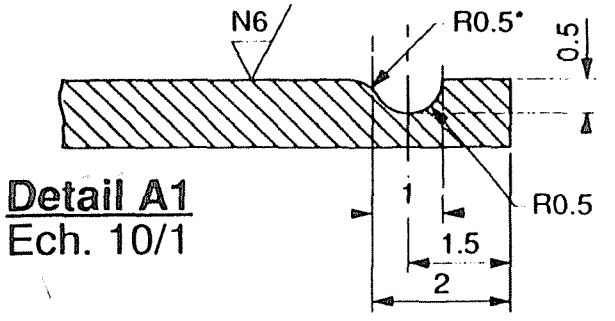


**Detail A1**
Ech. 10/1

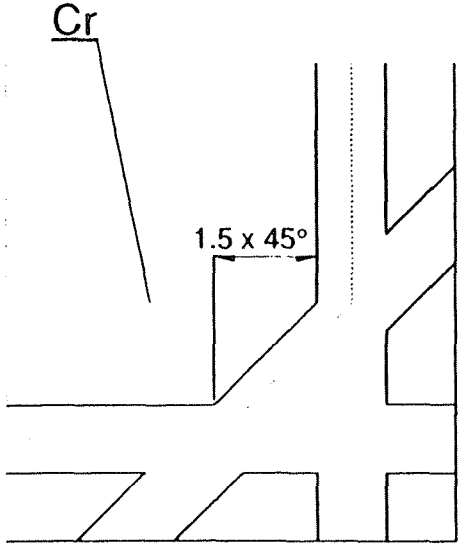


**Detail A3**
Ech. 10/1

*: ATTENTION : arrondi qualité N6
Tolérances Générales ±0.1

200 pièces

**Plan pour soumission**

Attention ! Ce plan est une réduction
il n'est pas à l'échelle
Dimensions en mm

| | | | | |
|---|---|---|---|---|
| Plaque ép.1 x 50 x 50 | | Céramique "Rubalit" 97%Alumine | | |
| DESCRIPTION | Pos | MATIERE | OBSERVATIONS | |
| ENSEMBLE | | S/ENSEMBLE | | |
| PLAQUE D'ELECTRODE | ECH SCALE 2/1 (10/1) | | N.41 | DATE |
| | | DESSINE | PETIT P | 3/4/92 |
| | | CONTROLE | | |
| | | VU | | |
| | | REMPLACE | | |
| | | LHC-RD5-M1-1051-2 | | |

Fig. 3 a)

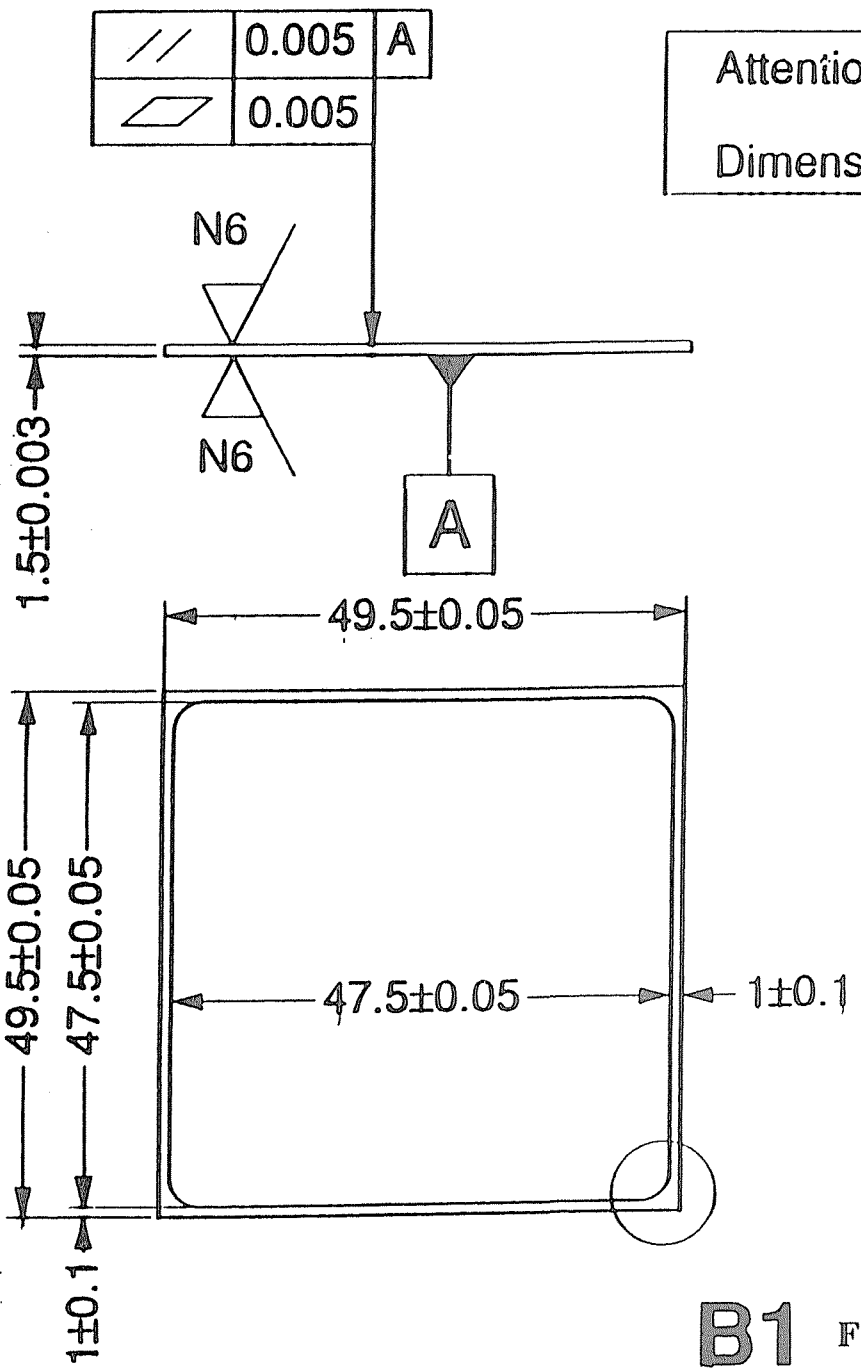


Attention ! Ce plan est une réduction
il n'est pas à l'échelle
Dimensions en mm

## Detail B1
Ech. 10/1

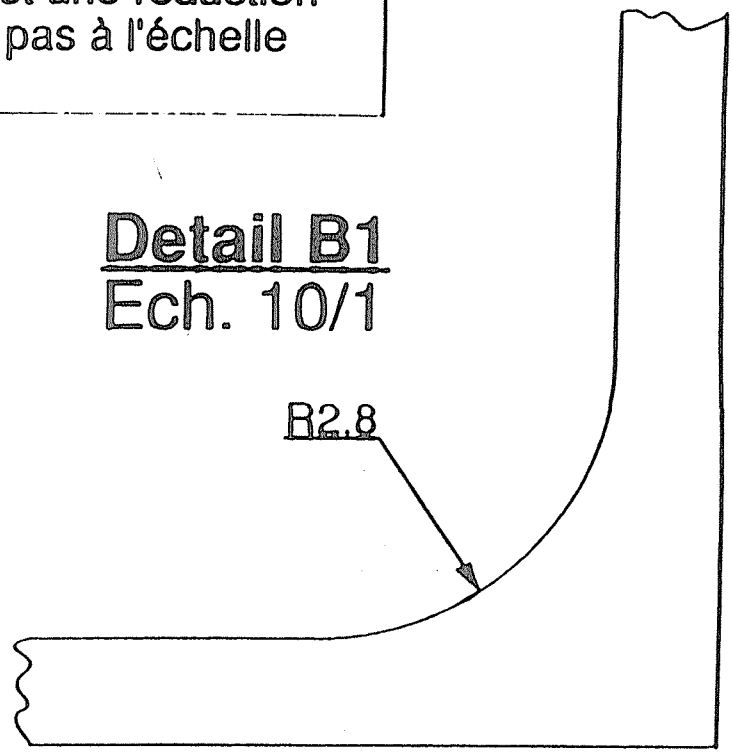


Tolérances Générales ±0.1

100 pièces

## Plan pour soumission

| | | | | | |
|---|---|---|---|---|---|
| Plaque ép.1.5 x 50 x 50 | | | Céramique "Rubalit" 97%Alumine | | |
| DESCRIPTION | POS | MATIERE | OBSERVATIONS | | |
| ENSEMBLE | | | S/ENSEMBLE | | |
| | | | | NOM | DATE |
| ENTRETOISE D'ELECTRODE | | | ECH. SCALE 2/1 (10/1) | DESSINE | PETIOT P 3/4/92 |
| | | | | CONTROLE | |
| | | | | VU | |
| | | | | REMPLACE | |
| ORGANISATION EUROPEENNE POUR LA RECHERCHE NUCLEAIRE | | | | LHC-RD5-M1-1050 -3 | |

B1 Fig. 3 b)

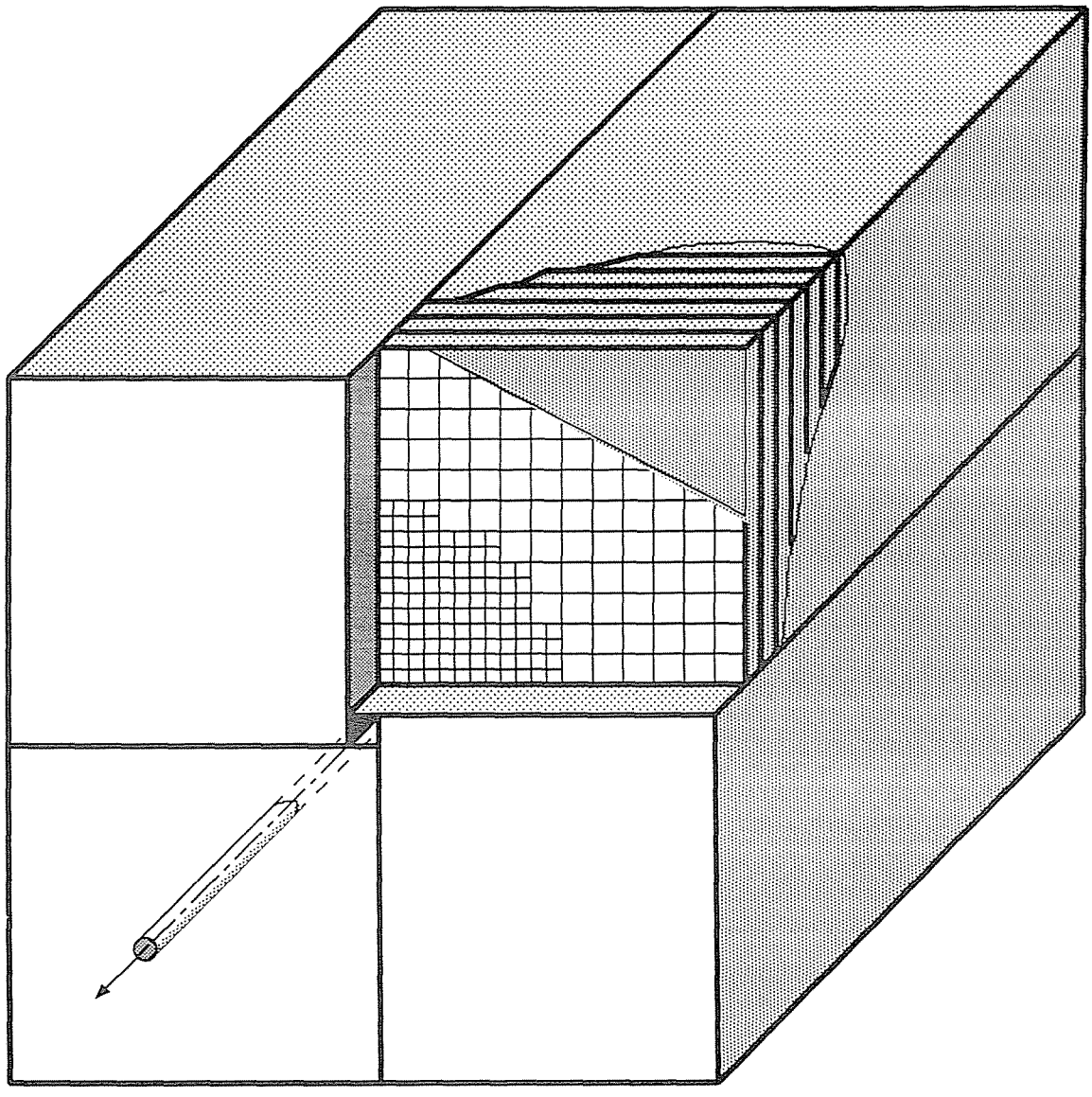

Fig. 4

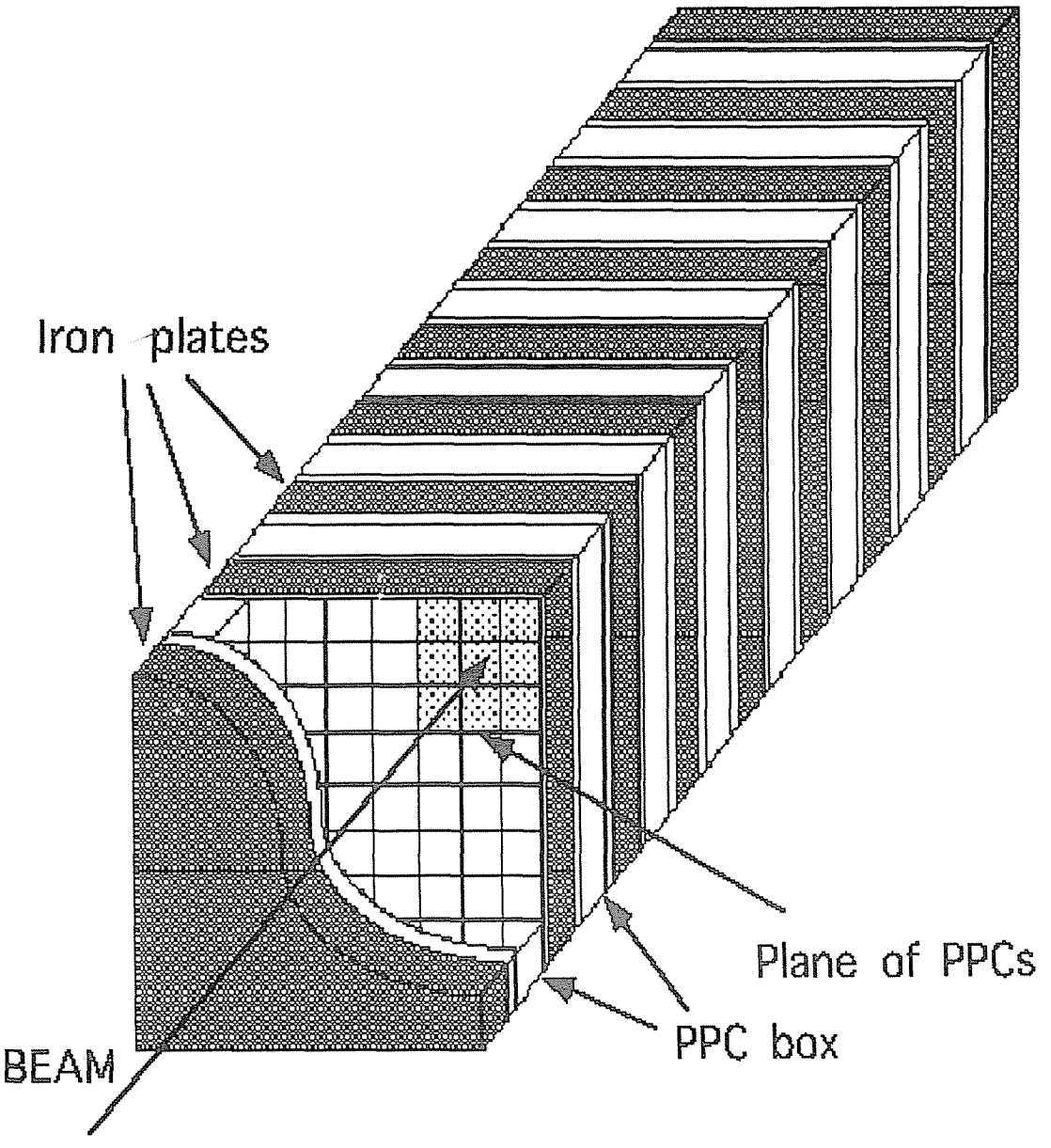


Fig. 5

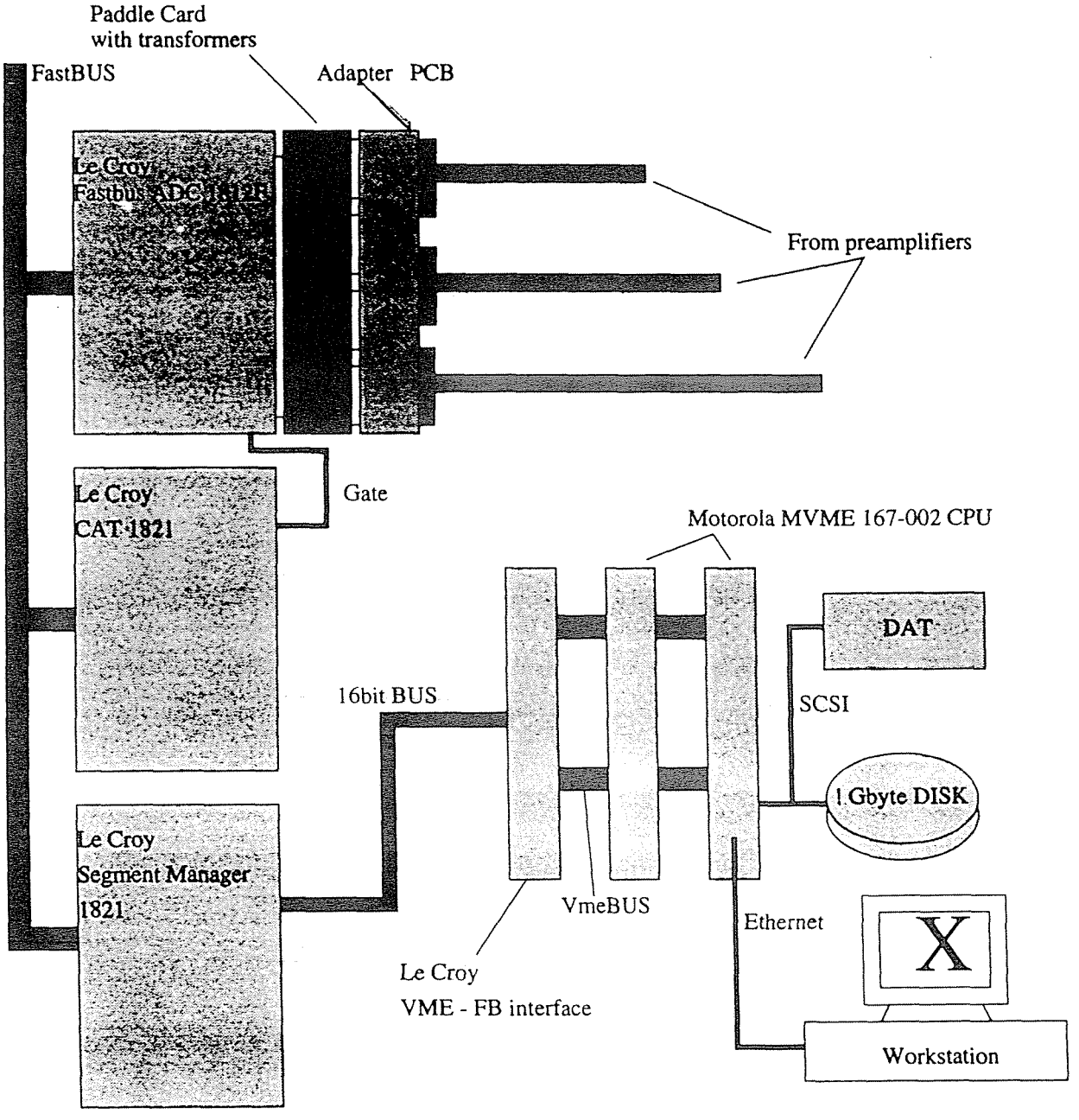
Paddle Card
with transformers
FastBUS
Adapter PCB
Le Croy
Fastbus ADC
From preamplifiers
Gate
Le Croy
CAT 1821
Motorola MVME 167-002 CPU
DAT
16bit BUS
SCSI
1 Gbyte DISK
Le Croy
Segment Manager
1821
VmeBUS
Ethernet
X
Le Croy
VME - FB interface
Workstation

**Fig. 6**

## a. $CO_2$ 5300 V

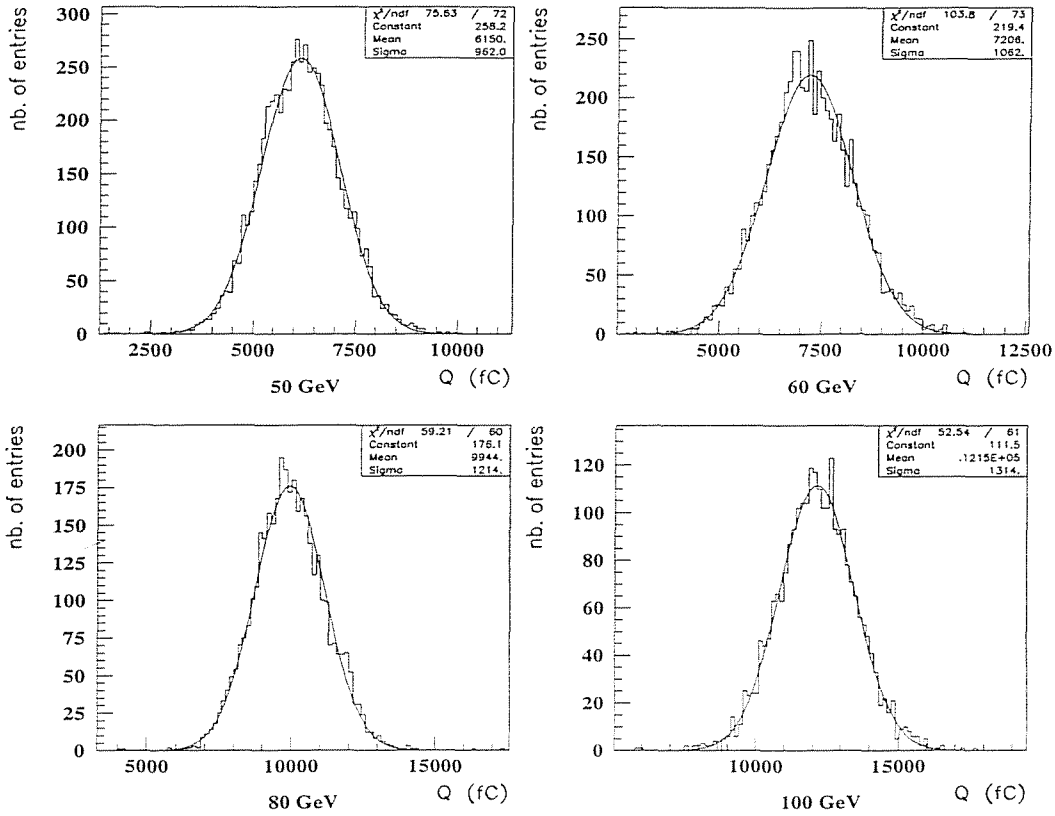


## b. $CO_2/CF_4$ (20/80) 5600 V

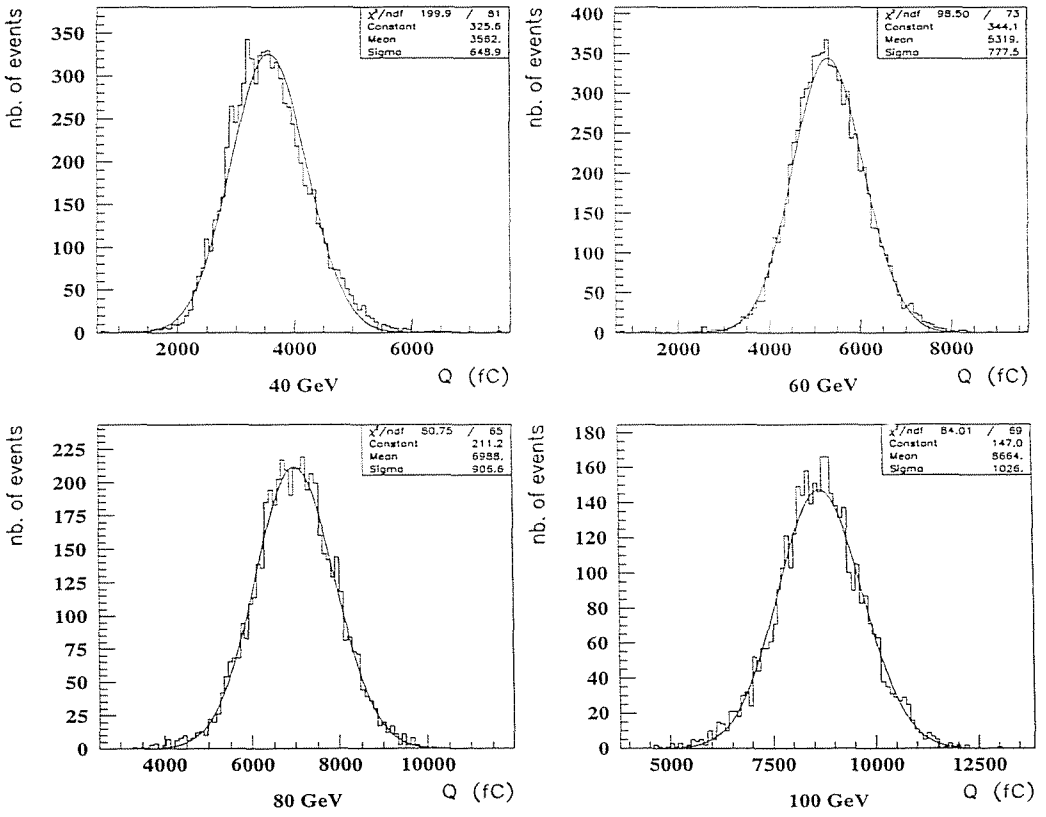


**Fig. 7**

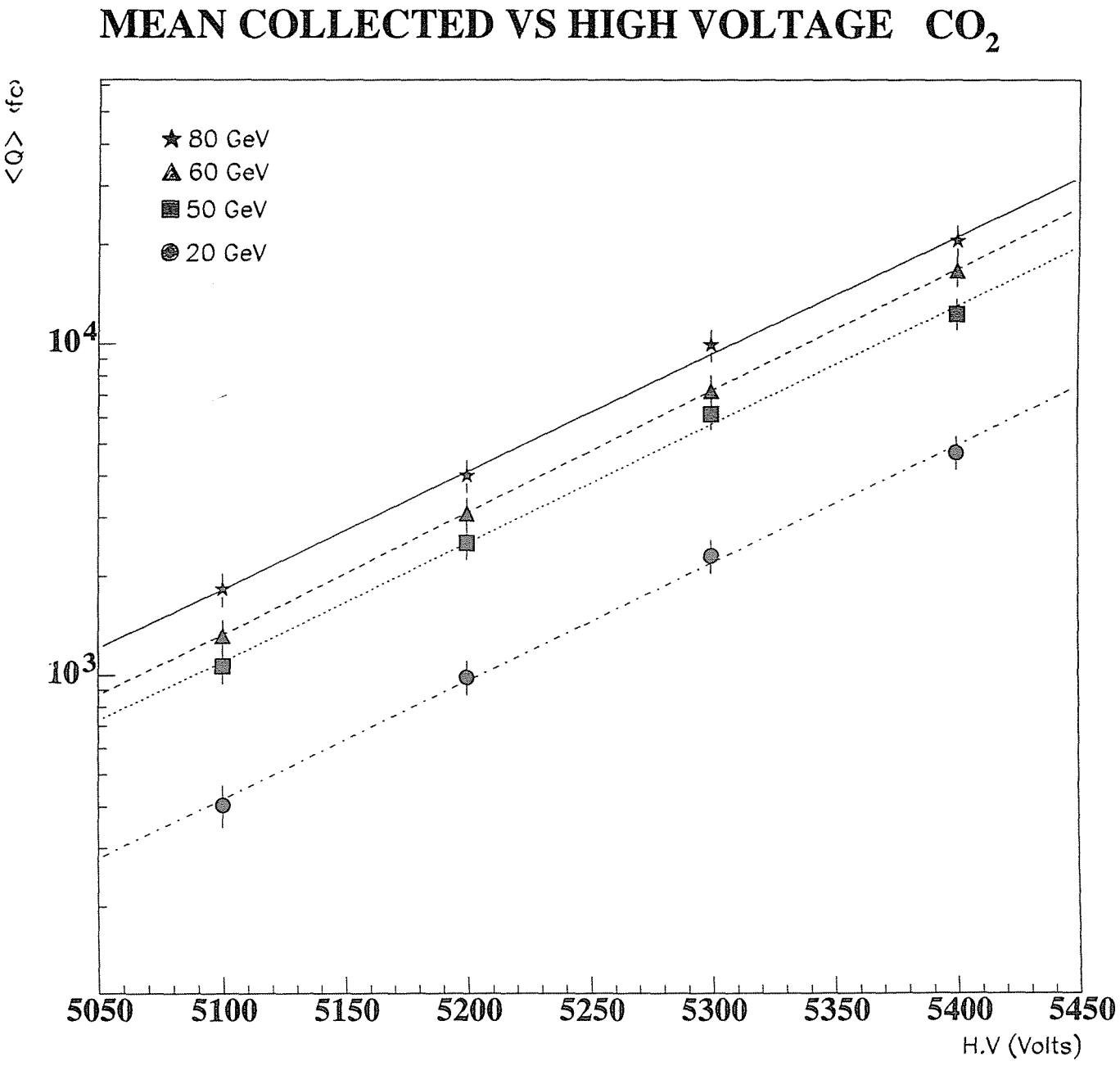
MEAN COLLECTED VS HIGH VOLTAGE $CO_2$
<Q> (fc)
80 GeV
60 GeV
50 GeV
20 GeV
$10^4$
$10^3$
5050
5100
5150
5200
5250
5300
5350
5400
5450
H.V (Volts)

**Fig. 8**

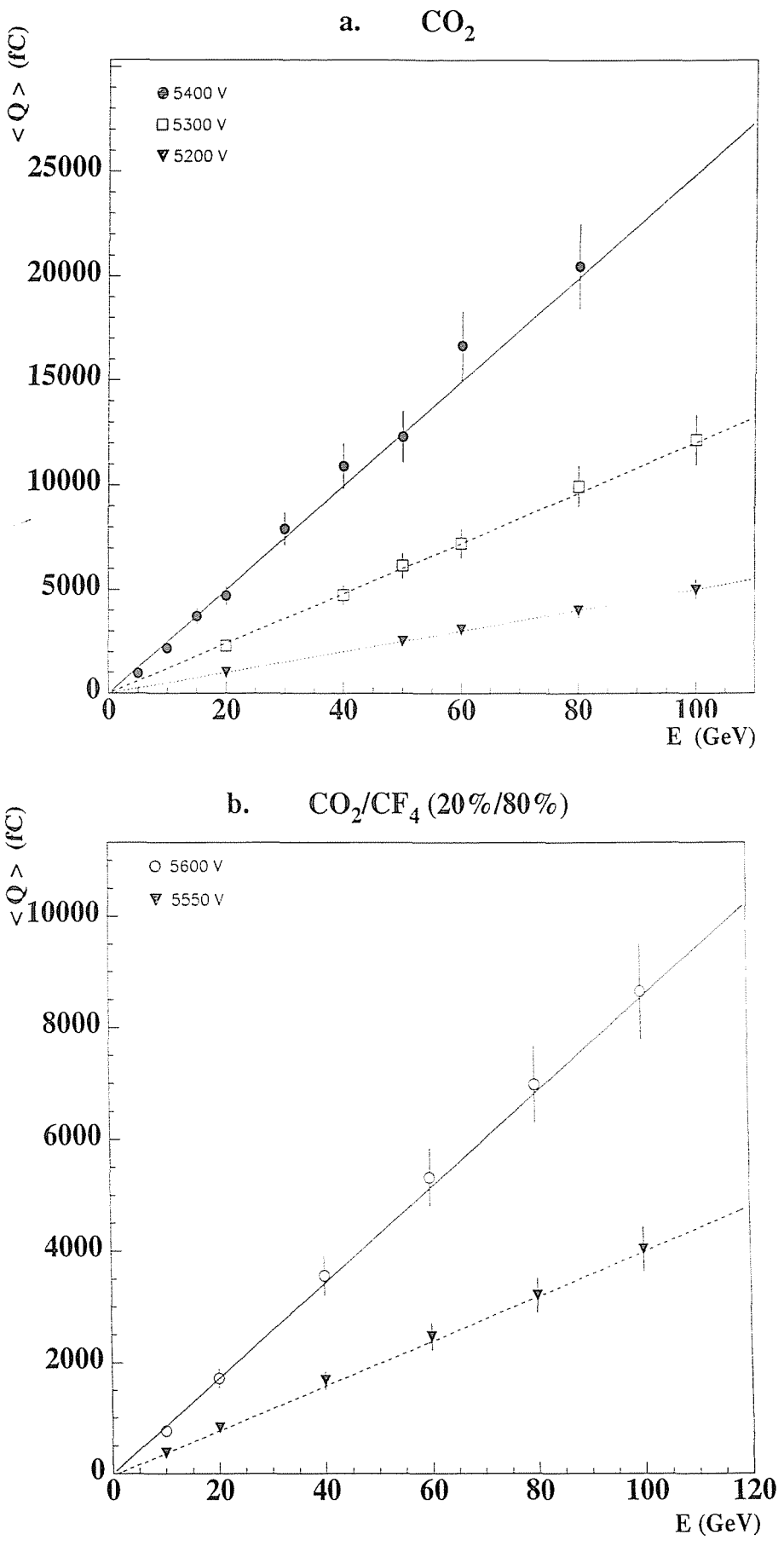
a. $CO_2$
< Q > (fC)
5400 V
5300 V
5200 V
25000
20000
15000
10000
5000
0
0
20
40
60
80
100
E (GeV)
b. $CO_2/CF_4$ (20%/80%)
< Q > (fC)
5600 V
5550 V
10000
8000
6000
4000
2000
0
0
20
40
60
80
100
120
E (GeV)

**Fig. 9**

a. $CO_2$

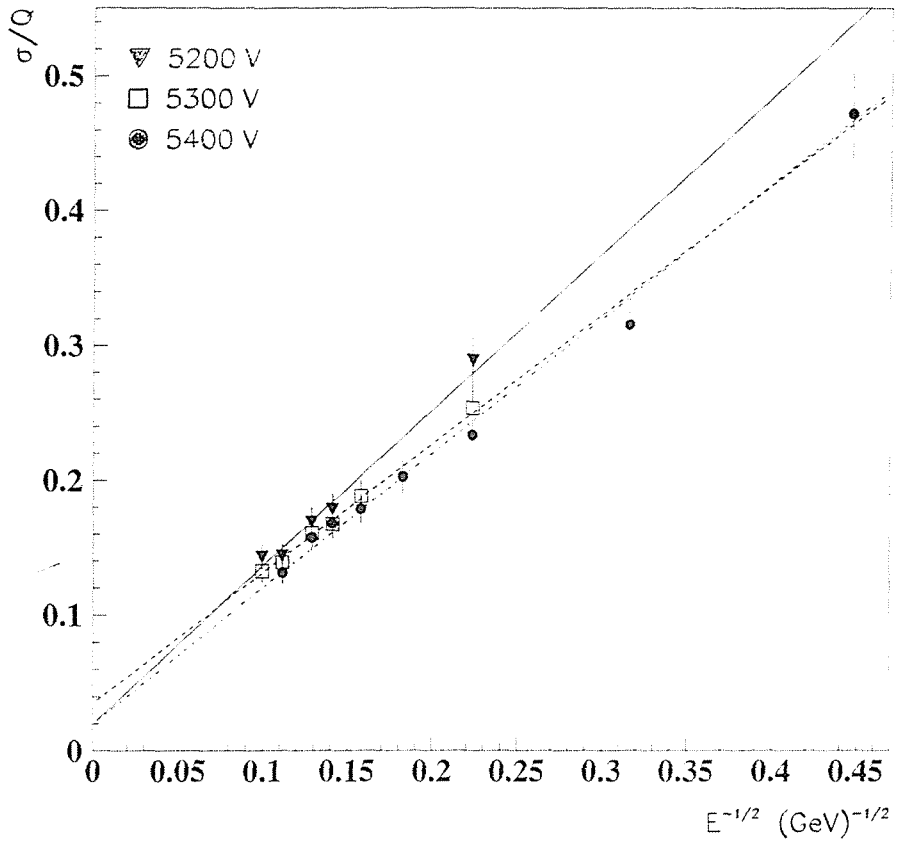


b. $CO_2/CF_4$ (20%/80%)

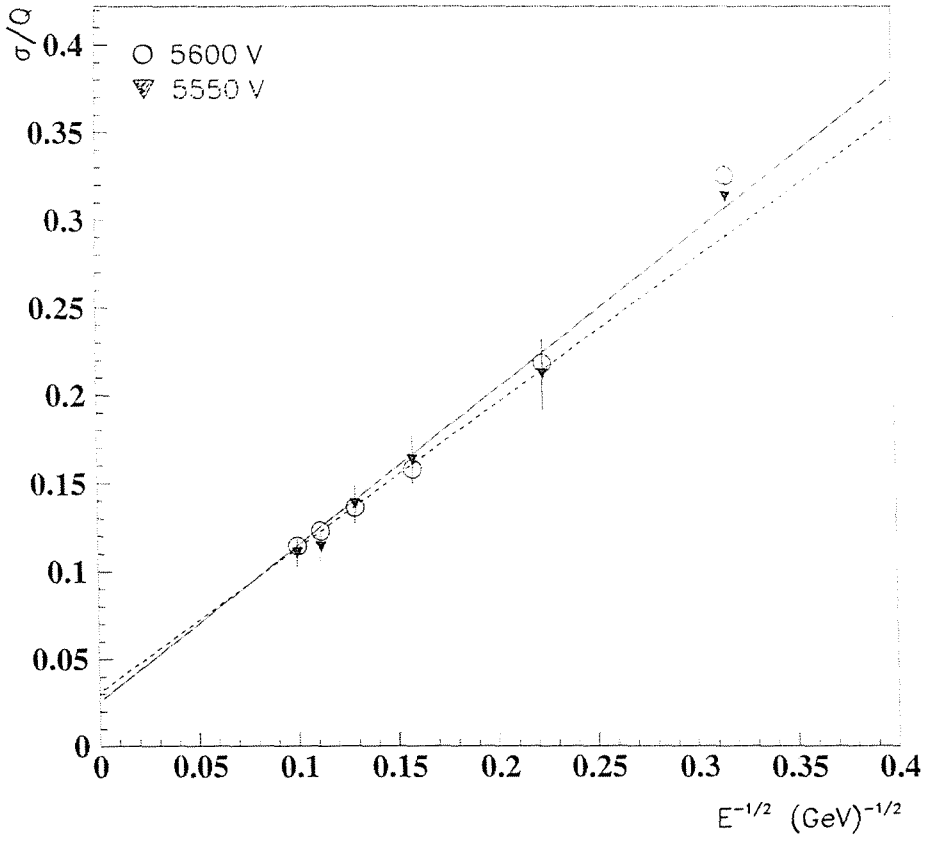


**Fig. 10**

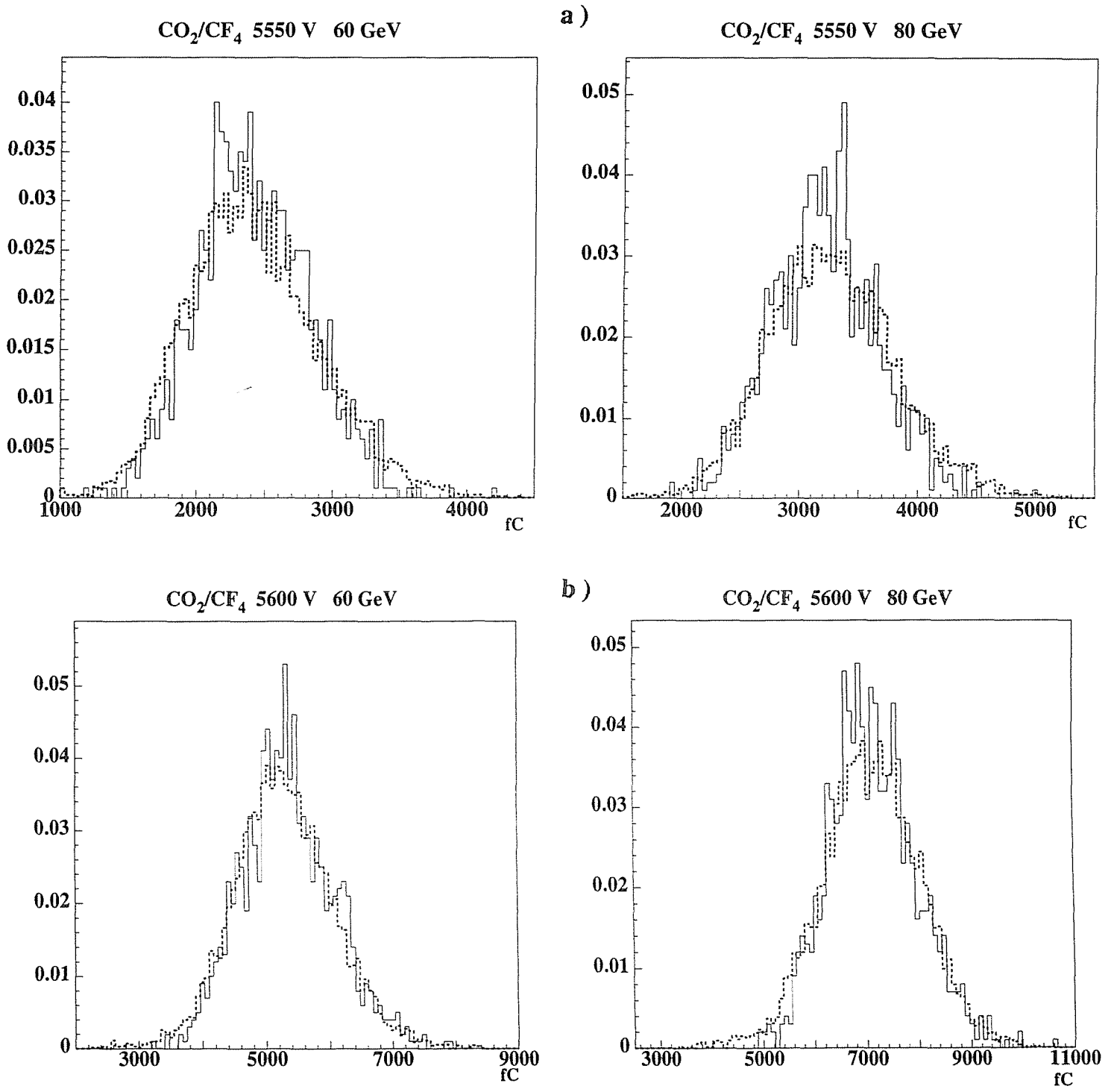
a )
$CO_2/CF_4$ 5550 V 60 GeV
$CO_2/CF_4$ 5550 V 80 GeV
b )
$CO_2/CF_4$ 5600 V 60 GeV
$CO_2/CF_4$ 5600 V 80 GeV
fC

**Fig. 11**

a. $CO_2/CF_4$ (20%/80%) 5550V

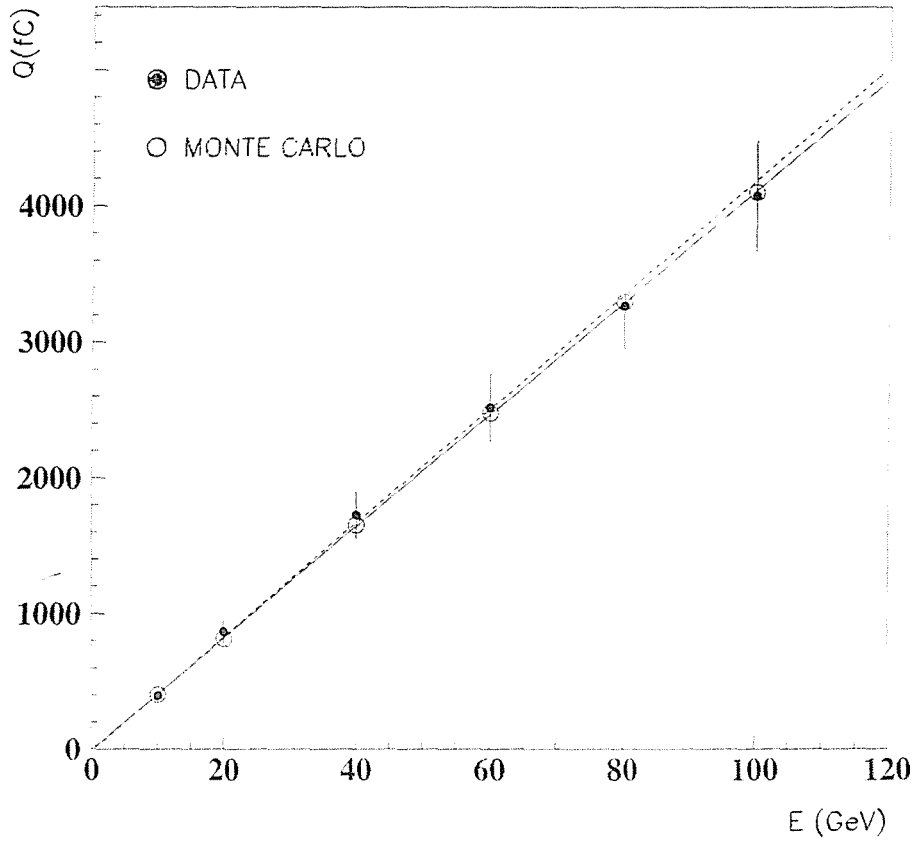


b. $CO_2/CF_4$ (20%/80%) 5600V

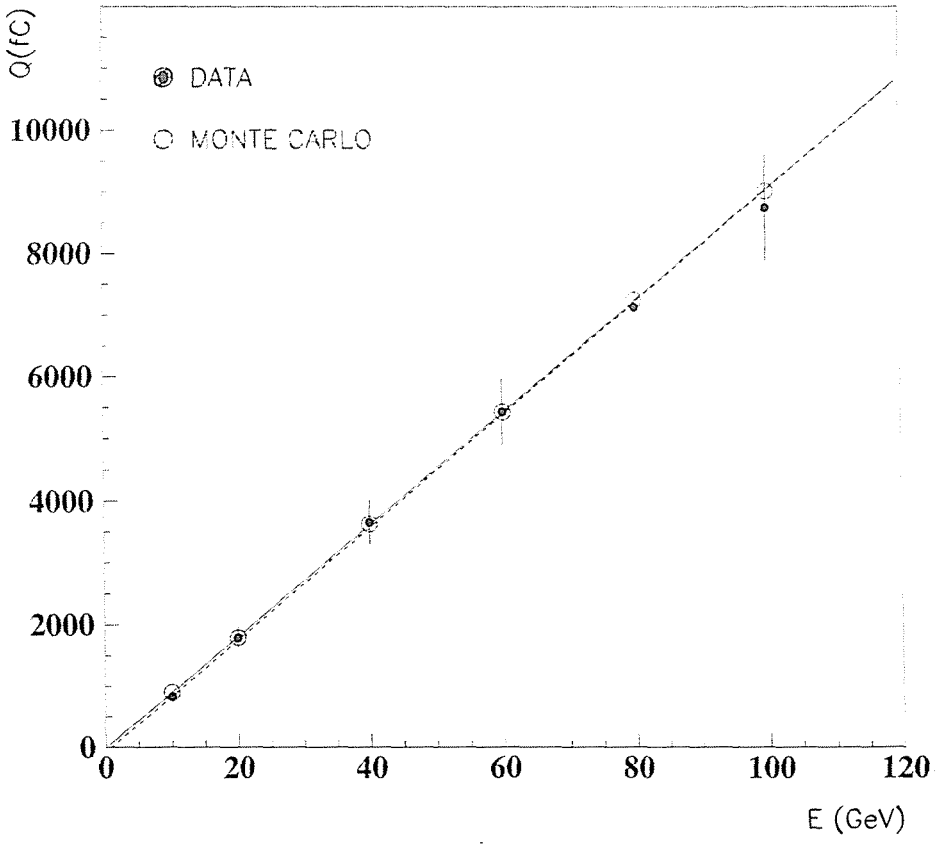


**Fig. 12**

a. $CO_2/CF_4$ (20%/80%) 5550 V

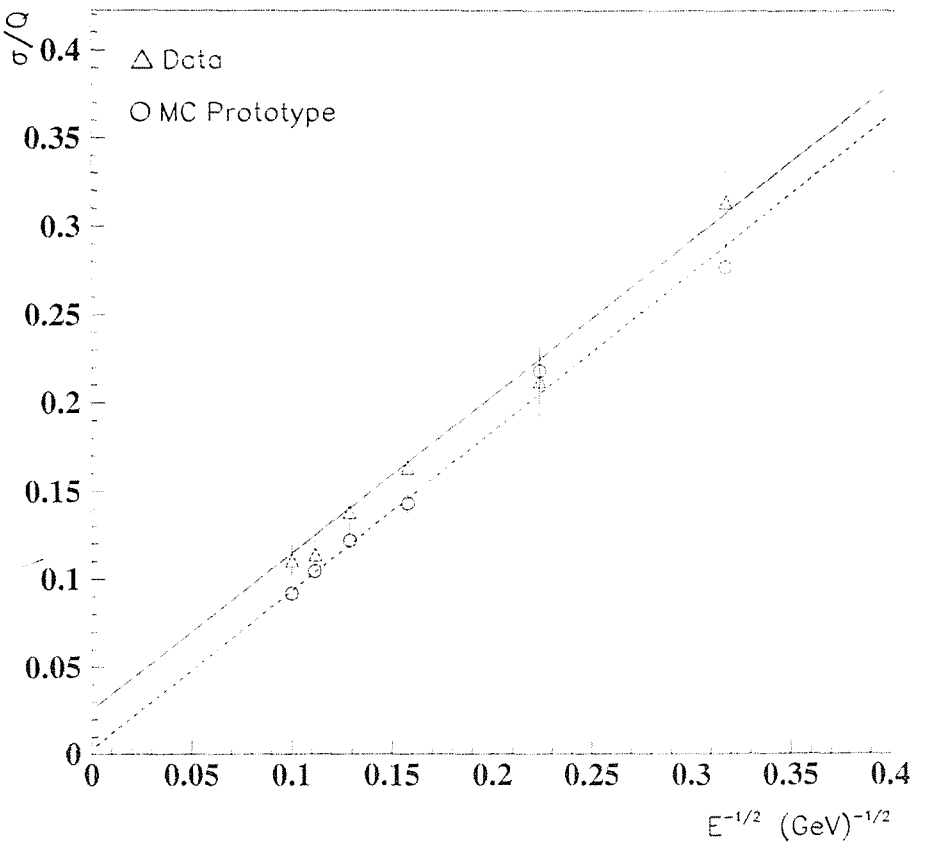


a. $CO_2/CF_4$ (20%/80%) 5600V

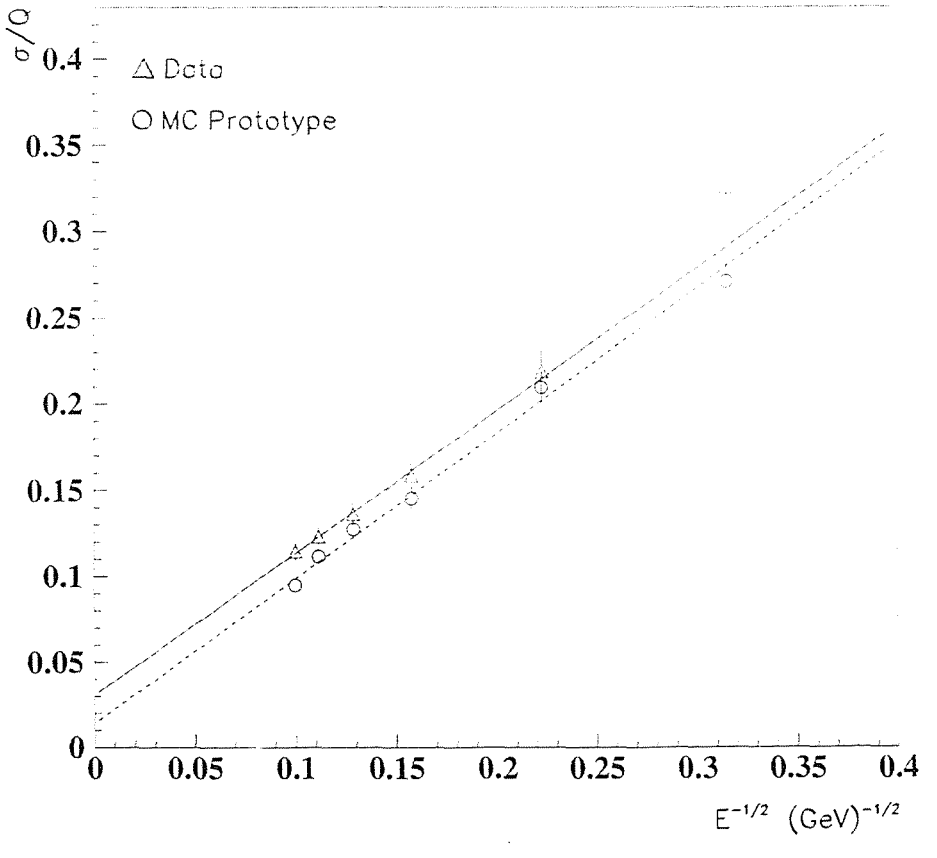


**Fig. 13**